Measurement of the collision rate coefficients between atmospheric ions and multiply charged aerosol particles in the CERN CLOUD chamber

Joschka Pfeifer[1,7], Naser G. A. Mahfouz[2,3,4], Benjamin C. Schulze[5], Serge Mathot[1], Dominik Stolzenburg[6], Rima Baalbaki[6], Zoé Brasseur[6], Lucia Caudillo[7], Lubna Dada[8], Manuel Granzin[7], Xu-Cheng He[6,9], Houssni Lamkaddam[8], Brandon Lopez[3], Vladimir Makhmutov[10,11], Ruby Marten[8], Bernhard Mentler[12], Tatjana Müller[7], Antti Onnela[1], Maxim Philippov[10], Ana A. Piedehierro[9], Birte Rörup[6], Meredith Schervish[2,13], Ping Tian[14], Nsikanabasi S. Umo[15], Dongyu S. Wang[8], Mingyi Wang[5], Stefan K. Weber[1,7], André Welti[9], Yusheng Wu[6], Marcel Zauner-Wieczorek[7], Antonio Amorim[16], Imad El Haddad[8], Markku Kulmala[6], Katrianne Lehtipalo[6,9], Tuukka Petäjä[6], António Tomé[17], Sander Mirme[18,19], Hanna E. Manninen[1], Neil M. Donahue[2,3], Richard C. Flagan[5], Andreas Kürten[7], Joachim Curtius[7], Jasper Kirkby[1,7]

[1]CERN, 1211 Geneva, Switzerland
[2]Center for Atmospheric Particle Studies, Carnegie Mellon University, Pittsburgh, PA 15213, USA
[3]Department of Chemical Engineering, Carnegie Mellon University, Pittsburgh, PA 15213, USA
[4]Program in Atmospheric and Oceanic Sciences, Princeton University, Princeton, NJ 08544, USA
[5]Department of Environmental Science and Engineering, California Institute of Technology, Pasadena, CA 91125, USA
[6]Institute for Atmospheric and Earth System Research (INAR)/ Physics, Faculty of Science, University of Helsinki, Helsinki, FI-00560, Finland
[7]Institute for Atmospheric and Environmental Sciences, Goethe University Frankfurt, 60438 Frankfurt am Main, Germany
[8]Laboratory of Atmospheric Chemistry, Paul Scherrer Institute (PSI), 5232 Villigen-PSI, Switzerland
[9]Finnish Meteorological Institute, 00560 Helsinki, Finland
[10]P.N. Lebedev Physical Institute of the Russian Academy of Sciences, 119991 Moscow, Russian Federation
[11]Moscow Institute of Physics and Technology (National Research University), 117303 Moscow, Russian Federation
[12]Institute for Ion and Applied Physics, University of Innsbruck, 6020 Innsbruck, Austria
[13]Department of Chemistry, University of California, Irvine, CA 92697, USA
[14]Beijing weather modification center, Beijing, 100089, China
[15]Institute of Meteorology and Climate Research (IMK-AAF), Karlsruhe Institute of Technology (KIT), 76344 Eggenstein-Leopoldshafen, Germany
[16]CENTRA and FCUL, University of Lisbon, 1749-016 Lisbon, Portugal
[17]IDL-Universidade da Beira Interior, Rua Marquês D"Ávila e Bolama, 6201-001 Covilhã, Portugal
[18]Institute of Physics, Unversity of Tartu, Estonia
[19]Airel Ltd., 50411, Tartu, Estonia

Correspondence to: Joschka Pfeifer (joschka.pfeifer@cern.ch)

Abstract. Aerosol particles have an important role in Earth's radiation balance and climate, both directly and indirectly through aerosol–cloud interactions. Most aerosol particles in the atmosphere are weakly charged, affecting both their collision rates with ions and neutral molecules, as well as the rates by which they are scavenged by other aerosol particles and cloud droplets. The rate coefficients between ions and aerosol particles are important since they determine the growth rates and lifetimes of ions and charged aerosol particles, and so may influence cloud microphysics, ~~dynamics~~dynamics, and aerosol processing. However, despite their importance, very few experimental measurements exist of charged aerosol collision rates under

atmospheric conditions, where galactic cosmic rays in the lower troposphere give rise to ion pair concentrations of around 1000 cm^{-3}. Here we present measurements in the CERN CLOUD chamber of the rate coefficients between ions and small (<10 nm) aerosol particles containing up to 9 elementary charges, *e*. We find the rate coefficient of a singly charged ion with an oppositely charged particle increases from 2.0 (0.4-4.4) $\times$ 10^{-6} cm^3 s^{-1} to 30.6 (24.9-45.1) $\times$ 10^{-6} cm^3 s^{-1} for particles with charges of 1 *e* to 9 *e*, respectively, where the parentheses indicate the $\pm 1\sigma$ uncertainty interval. Our measurements are compatible with theoretical predictions and show excellent agreement with the model of Gatti and Kortshagen (2008).

1 Introduction

Atmospheric aerosols play an important, yet uncertain, role in Earth's radiative balance. The largest source of uncertainty in current climate projections is due to aerosols and their interactions with clouds (Intergovernmental Panel on Climate Change, 2014a). For new atmospheric particles to be climatically relevant, they must grow to sizes above approximately 50 nm where they can constitute cloud condensation cloud nuclei, CCN (Intergovernmental Panel on Climate Change, 2014b). During this growth — and especially in the size range below 10 nm where they are highly mobile — new particles are highly susceptible to loss from scavenging by pre-existing larger particles. Consequently, the balance between growth rates due to collisions with condensable vapours and the loss rates to pre-existing particles ~~the balance between loss rates to pre-existing particles and growth rates (due to collisions with condensable vapours)~~ plays a central role in determining the fraction of new particles that reach CCN sizes and influence climate (Marten et al., 2022; Mahfouz and Donahue, 2021a; Kulmala et al., 2017).

Electric charge plays an important role in new particle formation by stabilising the embryonic molecular clusters against evaporation (Kirkby et al., 2016, 2011; Turco et al., 1998). The presence of charges also enhances the growth rate of molecular clusters (He et al., 2021) and newly formed particles (Stolzenburg et al., 2020). However, charge can also enhance particle losses to pre-existing particles of opposite polarity (Mahfouz and Donahue, 2021a, b), or even neutral particles via Van der Waals enhancement. To understand the role of charge in the formation of CCN requires a quantitative understanding of the charge state of the atmospheric aerosol. This, in turn, requires knowledge of particle–particle and ion–particle rate coefficients under atmospheric conditions. Previous studies have for the most part considered collisions between particles or molecules where only one is charged (e.g., Dépée et al., 2021; He et al., 2021). Yet, particles with larger numbers of charges are found in the atmosphere (e.g., Tinsley et al., 2000), and in many laboratory experiments, especially in generation of calibration aerosols.

In the atmosphere, high charges exist on aerosol particles and hydro-meteors in thunderclouds, but also on aerosol particles during fair weather resulting from the evaporation of charged cloud droplets (Tinsley et al., 2000). The excess charge on aerosol particles in cloud systems is expected to enhance "electro-scavenging" whereby charged particles are lost to bigger droplets of opposite sign (Tinsley et al., 2000; Guo and Xue, 2021). Simulations by Guo and Xue (2021) show that multiply charged particles can have a significant influence on cloud lifetime. Charge is transferred from smaller particles to larger droplets when they collide, which increases the growth rate of multiply charged CCN compared with their neutral counterparts

(Guo and Xue, 2021). Moreover, there exists a charge gradient on droplets in a cloud, where droplets have positive charges atop of the cloud and negative charges at the bottom of it (Zhou and Tinsley, 2007). Quantifying the rate coefficients between

75 available atmospheric ions and charged particles can thus inform models and understanding of cloud systems.

In this study, we report measurements of the rate coefficients between ions and charged small (<10 nm) aerosol particles containing up to 9 elementary charges, e, of opposite charge. Such highly overcharged particles below 10 nm are extremely rare in the atmosphere, but they provide an important and sensitive constraint for theory. Knowledge of ion–aerosol rate coefficients is important to infer the particle steady-state charge distribution and to model the dynamics of aerosol

80 populations. In particular, the particle steady-state charge distribution is essential for mobility-based size distribution measurements, for example when using differential mobility analysers (Kangasluoma and Kontkanen, 2017; Zeleny, 1900; Winklmayr et al., 1991; Flagan, 1998). To estimate the rate coefficients under atmospheric conditions, theoretical models based on first principles are often used. Chief amongst the current paradigms to estimate the charge-enhanced collisions are models based on the limiting-sphere model as detailed (and extended) by López-Yglesias and Flagan (2013) and references

85 therein (e.g., Fuchs, 1963; Hoppel and Frick, 1986). In the limiting-sphere model, the motion between particles that are far from each is described by continuum mechanics, but within a limiting-sphere radius, their motion is described by free molecular mechanics; at the limiting-sphere radius, both motion fluxes are set to be equal.

An alternative approach to limiting-sphere models are calculations based on mean first-time passage and dimensional analysis as discussed by Gopalakrishnan and Hogan (2012) and subsequent studies (e.g., Ouyang et al., 2012; Gopalakrishnan

90 et al., 2013; Chahl and Gopalakrishnan, 2019; Suresh et al., 2021). Gopalakrishnan and Hogan (2012) question the validity of limiting-sphere models in the presence of potential interactions and argue their long-standing success is due to the fact that it "can be fit" to experimental data, but not necessarily "agree" with said data (Gopalakrishnan and Hogan, 2012). In their recent studies, Tamadate et al. (2020a, b) show that a hybrid modelling approach connecting the continuum regime (outside the limiting sphere) with molecular dynamics (MD; inside the limiting sphere) simulations can achieve good agreement with some

95 laboratory experiments. Compared with limiting sphere simulations, continuum–MD simulations contain more detailed processes; chemical structures of the colliding entities are considered, as well as changes in translational, rotational and vibrational degrees of freedom (Tamadate et al., 2020a, b).

Gatti and Kortshagen (2008) propose a linear combination of three regimes (continuum, molecular, and transition) to construct a simple analytical model of rate coefficients. By conducting MD simulations between particles of diameters 10–

100 1000 nm and gas pressures 10^{-5}–10^5 Pa, Gatti and Kortshagen (2008) show that in the low- and high-pressure limits, results converge onto the limiting-sphere model and hydrodynamic (molecular) limit, respectively. In the transition regime, they find the limit-sphere model underpredicts the collision rates by up to 500 %. As such, the authors propose a weighted linear combination of the three regimes, accounting for three-body trapping in the transition regime. When using the proposed analytical model by Gatti and Kortshagen (2008), as reformulated by Gopalakrishnan and Hogan (2012), we find that it shows

105 the best agreement with our experimental results presented in this study.

We measure the rate coefficients of singly charged ions with multiply charged aerosol particles under atmospheric conditions in the CERN CLOUD chamber. We use an electrospray aerosol generator to generate multiply charged particles of around 10 nm diameter carrying positive charges. The particles are exposed with an X-ray source for control experiments with singly charged and neutral particles. The evolution of most relevant properties of the particles are monitored with a comprehensive suite of instruments that continuously sample air from the CLOUD chamber. The positive charge on the particles gradually decays due to collisions with negative ions produced by galactic cosmic rays traversing the chamber. From our measurements, we derive the ion–aerosol rate coefficients for particles carrying up to nine positive charges.

Previously, experimentally determined ion–aerosol rate coefficients for multiply charged particles have been reported only for aerosol particles larger than 100 nm (e.g., Dépée et al., 2021). For particles smaller than 10 nm, only singly charged ion–ion recombination coefficients have been experimentally reported (Franchin et al., 2015). The collision rate of uncharged monomers with singly charged aerosol particles below 2 nm size has been measured by He et al. (2021). Owing to the dearth of experimental measurements for multiply charged particles, Tamadate et al. (2020b) compared their modelled coefficients with measured multiply charged PEG particles from an electrospray. To our knowledge, our study represents the first experimental measurement of ion–aerosol rate coefficients for multiply-charged, small (<10 nm) aerosol particles under atmospheric conditions. We compare our results to several theoretical predictions and find they are generally compatible, while identifying some models that show excellent agreement.

Table 1. Parameter list

Parameter	Description	Units
I_{calc}	Calculated current in NAIS	A
H	Instrument apparatus matrix of NAIS	A cm^3
$\boldsymbol{\phi} = (\phi_1, \phi_2, \dots \phi_{25})$	Lognormal distribution coefficients	cm^{-3}
$\widehat{\Omega}$	Lognormal probability density function	
$\Omega_\pm$	Calculated singly charged (positive/negative) number distribution	cm^{-3}
Ω_0	Calculated neutral number distribution	cm^{-3}
I_{meas}	Measured current in NAIS (vector representing 25 channels)	A
t	Time in seconds; t_{end} is the time at the end of the decay stage	s
j	Number of charges (i.e., charging state)	
$\widehat{\omega_j}$	Assumed probability density function for charging state j	
γ_j	The total number concentration of particles in a given charging state j	cm^{-3}
ω_j	Calculated number distribution at charging state j	cm^{-3}
Z_p	Electric mobility	cm^2 V^{-1} s^{-1}
q	Elementary charge constant	C
C_{c}	Cunningham's slip correction factor	
d_{p}	Particle diameter	nm
η	Particle viscosity	Pa s
k	Loss rate constant	s^{-1}
k_{wall}	Wall loss rate coefficient	s^{-1}
C_{wall}	Wall loss rate proportionality factor	cm^{-1} s$^{-1/2}$
k_{dil}	Dilution loss rate coefficient	s^{-1}
D_{p}	Particle diffusion coefficient	cm^2 s^{-1}
β_j	Rate coefficient between an ion and a particle with charging state j	cm^3 s^{-1}
K	Coagulation coefficient between neutral particles	cm^3 s^{-1}
CS	Coagulation sink to neutral particles	cm^{-3} s^{-1}
L_j	Total loss rate (wall loss, dilution loss, and coagulation sink to neutral particles)	cm^{-3} s^{-1}
$\breve{\sigma}_j$	Modified Coulombic enhancement between an ion and a particle with charging state j	
σ_j	Normalized $\breve{\sigma}_j$	
$\omega_{j,0}$	Number distribution at charging state j at start of decay stage	cm^{-3}
$\omega_{j,\infty}$	Instrument background number distribution at charging state j	cm^{-3}

2 Methods

The overall goal of the experiments herein is to infer the rate coefficients between negative atmospheric ions and positively
overcharged small atmospheric aerosols. To achieve this, particles were produced using the CHARGE instrument (Sect. 2.1.2)
and injected into the CERN CLOUD chamber (Sect 2.1.1). A comprehensive suite of instruments (Sect. 2.1.4) is used to
monitor particles and charge states through the experiment to constrain and infer (Sect. 2.2) the ion-charged aerosol rate
coefficients.

2.1 Experimental approach

Our experimental approach follows the one documented by Dada et al. (2020). Below, we summarize key aspects of the overall
experimental approach that are most relevant to the subject of this study. The reader is invited to find more details about the
experimental setup in Dada et al. (2020).

2.1.1 CLOUD chamber

The Cosmic Leaving Outdoor Droplets (CLOUD) chamber at CERN is a 26.1 m^3 stainless steel container that enables aerosol
experiments to be performed under atmospheric conditions with very low contaminant levels (Kirkby et al., 2011; Pfeifer et
al., 2020). The chamber uses synthetic air from cryogenic nitrogen and oxygen (dilution flowrate during the experiments: 250
l min^{-1}). All parameters of the air in the chamber — such as temperature, relative humidity, UV light intensities and trace
vapours — can be controlled with high precision (Dias et al., 2017; Kupc et al., 2011). For experiments under neutral
(uncharged) conditions, an electric field of around 20 kV/m can be established with two electrodes, which sweeps charged
small ions from the chamber in under within 1 s. All experiments described here were carried out in dark conditions, that is,
no UV lamps were switched on. The relative humidity was maintained at 80 %, and ozone at 40 ppbv. The electrospray
generator used a dilute sulphuric acid solution in water. No other trace gases were added during the experiments.

2.1.2 CHARGE instrument

We developed the CHarged AeRosol GEnerator (CHARGE) electrospray instrument to obtainstudy multiply charged particles
under atmospheric conditions. Electrospray is used in various research fields to enable the generation of singly and multiply
charged particles (Sterling et al., 2011; Hogan and de la Mora, 2011; Marginean et al., 2008). By applying a strong voltage
gradient at the tip of a capillary, a liquid solution emerging from the capillary is drawn into a so-called Taylor cone. Highly
charged droplets stream from the tip of the Taylor cone. Once exposed to sub-saturated air, the charged droplets evaporate and
shrink until the repulsive electrostatic force causes them to break up into several multiply charged smaller droplets (Rayleigh,
1882; Smith et al., 2002). Following López-Herrera et al. (2004), we used electrospray solutions consisting of sulfuric acid
(0.02 wt. %) and purified water (0.98 wt. %) to generate positively charged particles using a positive voltage of 5200 V (Myhre
et al., 1998; Kebarle and Verkerk, 2009). CHARGE incorporated an X-ray ion generator along the path of the charged particles.

When switched on, this generated a highly concentrated bipolar ion distribution, thereby forcing the particles to their particle charge steady state. This way, multiply charged particles in one experiment could be directly compared to an otherwise
155 identical experiment performed with a particle distribution in charge steady state, presumably containing neutral and singly charged particles.
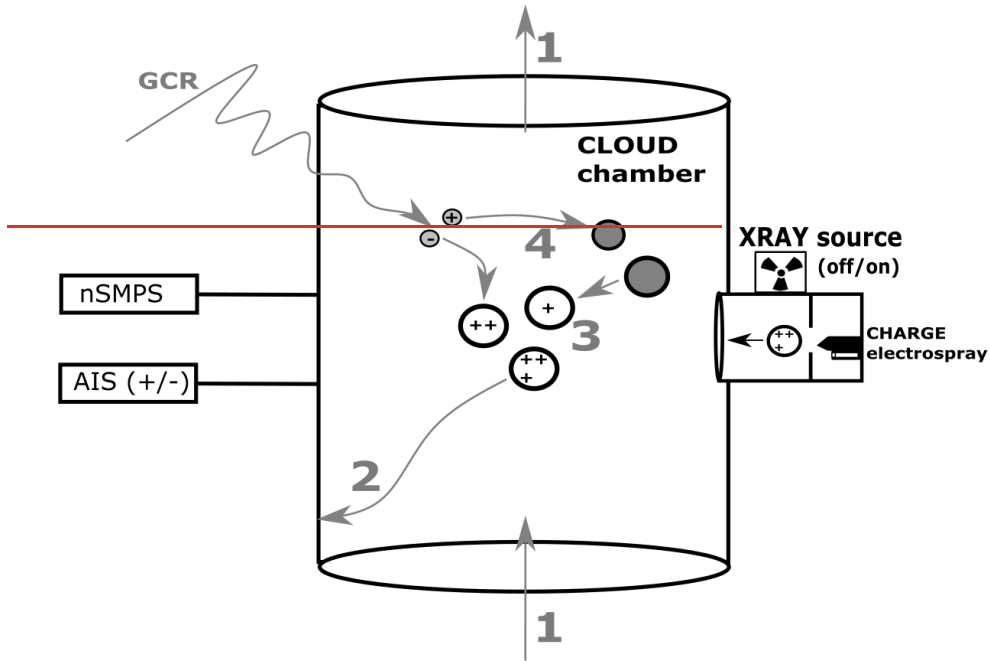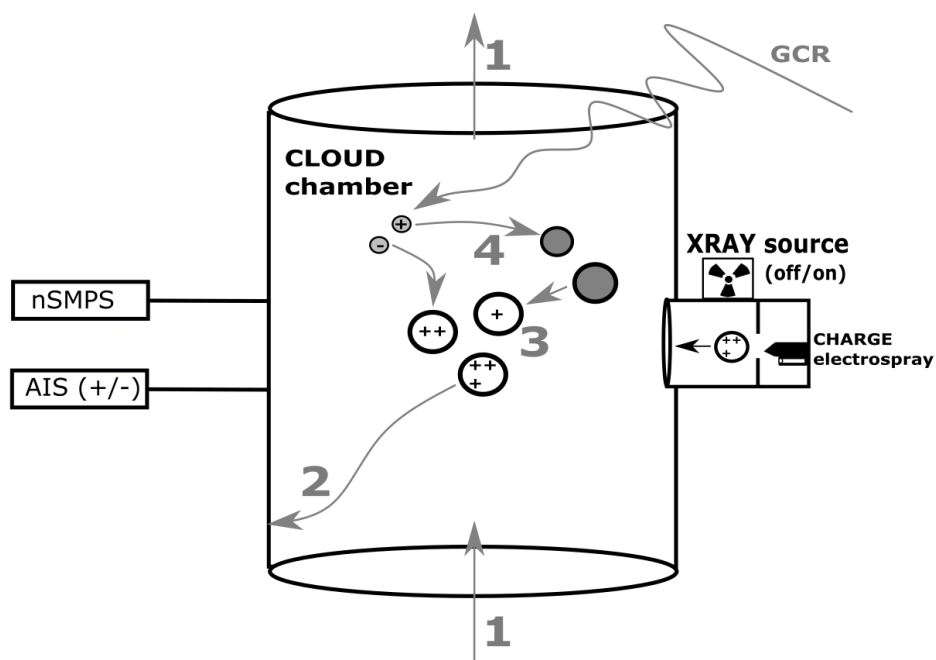
160 **Figure 1: Schematic representation of the experimental measurements.** Charged particles are produced by the CHARGE electrospray instrument (right). With the X-ray source switched off, charged particles enter the CLOUD chamber. With the X-ray source switched on, the particles are neutralised, i.e. have a steady-state charge distribution, before entering the CLOUD chamber. After an injection period of around 30 min, particle injection from CHARGE is switched off and the evolution of the particle charges during the "decay stage" is monitored by sampling instruments such as the nSMPS and AIS (left). The evolution of particle and ion charges in the chamber is analysed
165 as a function of the production and loss terms: (1) dilution loss, (2) wall loss, (3) ~~aerosol–aerosol collisions~~coagulation loss, (4) collisions of aerosols with ions produced by galactic cosmic rays.

2.1.3 Experimental overview

Figure 1 shows a schematic representation of the experiments reported in this study. We performed two distinct experiments: with and without X-ray. All experiments started with the injection of particles to the chamber from CHARGE; the number of

170 particles and their charge then decayed inside the chamber. During injection, we injected particles through a large-diameter tube (100 mm in diameter) at a high carrier flow rate of approximately 200 ~~l~~l min⁻¹. During the decay stage, we turned off all voltages and flows in CHARGE and observed the decay of the particle and ion distributions in the chamber. Since no more particles were added during this stage, the decay could be described by the production and loss terms shown in Figure 1 and

described in Sect. 2.2.3. Between experiments, we removed particles and ions by increasing the flow rate of the chamber and
175   the fan speed as well as turning on the high-voltage electrode grids to remove any remaining charged particles and ions.

2.1.4 Instrumentation and measurements

Relative humidity was measured with a Tunable Diode Laser system, TDL (Skrotzki, 2012). In addition, a chilled dew point
mirror (Edgetech Instruments) was used to derive the relative humidity utilizing water vapor pressure calculations (Murphy
and Koop, 2005). An ozone monitor (Thermo Electron Corporation Model 49C) was used to measure the ozone concentrations.
180   Sulfuric acid and gaseous compounds were measured with a Nitrate -Chemical Ionization–Atmospheric Pressure interface–
Time Of Flight mass spectrometer, CI-APi-TOF (Kürten et al., 2014). The instrument was operated and calibrated following
Kürten et al. (2012).

The total particle concentration (all charge states) was measured with a NanoScan Mobility Particle Sizer, nSMPS,
TSI, Model 3936 (Lehtipalo et al., 2014; Tritscher et al., 2013; Wiedensohler et al., 2012). The concentrations were compared
185   to the Scanning Mobility Particle Sizer (SMPS) results (Birmili et al., 1997; Wiedensohler, 1988). Total particle concentrations
for diameters larger than 2.5 nm (i.e., integrated over sizes above 2.5 nm) were obtained with a Particle Size Magnifier, PSM,
and a Condensation Particle Counter, CPC (Vanhanen et al., 2011; Liu et al., 2006).

Ion concentrations and the concentrations of charged particles with both polarities were measured with a Neutral
cluster and Air Ion Spectrometer (NAIS). To increase time resolution during the experiments, the NAIS was only used to
190   measure ions, that is, in "Ion Mode" (Manninen et al., 2009, 2016; Mirme and Mirme, 2013); as such, we refer to it as AIS
(Air Ion Spectrometer) for the rest of this study. Measurements from AIS were also compared with measurements from a nano-
radial DMA (Amanatidis et al., 2021).

To analyse the experiments, we primarily use data from the AIS (charged distribution) and from the nSMPS (total
distribution). All data have been converted from the measured mobility diameter to mass diameter (Ku and de la Mora, 2009;
195   Larriba et al., 2011). A comparable setup for chamber measurements of particle and ion distributions is described in more
detail by Dada et al. (2020).

2.2 Data analysis

2.2.1 AIS inversion

The AIS instrument is based on the design of electrical aerosol spectrometers (e.g., Flagan, 1998; Mirme et al., 2007). The
200   mobility analyser consists of multiple electrode rings to measure a differential ion distribution. Two analysers are arranged in
parallel with different polarities, where the sample flow (54 l min^{-1}) is split. This allows measuring particle distributions of
positive and negative polarity in parallel. While the instrument can also measure neutral particles by first filtering natural ions
(using an electric field) and afterwards charging the remaining neutral particles (with a corona needle), only charged particles
were measured in our experiments; as such, the ion filter and the corona needle were switched off. The AIS version used in

205   our experiments has 25 electrode channels. It is capable of measuring charged particles, cluster ions, and small ions in the mobility range from 3.2 to 0.0013 $cm^2 V^{-1} s^{-1}$ (Mirme and Mirme, 2013; Manninen et al., 2016).

       We follow the inversion function presented by Mirme and Mirme (2013) in analysing the AIS measurements However, we find that we need to adjust the approach in the case of multiply charged particles. First, we observed that the established (Mirme and Mirme, 2013) AIS inversion jumps suddenly during our experiments. However, we did not see this

210   jump in the measured current of the differential AIS channels. Furthermore, as shown in the next paragraphs, we want to describe the AIS measurement as a linear combination of several lognormal distributions with charge number j. The original inversion function used squares of cosine functions as basis functions to obtain a mobility distribution from the measured current. Accordingly, the measured current of the AIS channels would ultimately be described by several squares of cosine distributions, which afterwards would be fitted using several lognormal distributions. It thus seems more natural for our

215   measurements to use lognormal distributions to describe transfer functions instead; and it seems to be a more natural choice for lognormally distributed aerosol distributions. We additionally skip the Tikhonov regularization previously employed (Tikhonov, 1963; Mirme and Mirme, 2013) as our updated inversion seems not to benefit from it.

       The calculated current, I_{calc}, can be expressed as a product of the instrument apparatus matrix $\mathbf{H}$ and the lognormal distribution coefficients vector $\boldsymbol{\phi}$ as $I_{calc} = \mathbf{H}\boldsymbol{\phi}$ (Mirme and Mirme, 2013; Manninen et al., 2016). The matrix $\mathbf{H}$ is determined

220   through instrument calibration (Mirme and Mirme, 2013). In our case, $\boldsymbol{\phi}$ is a vector of the coefficients of 25 individual lognormal distributions, that is, it is a vector of the total number concentrations of each one of them. These 25 distributions correspond to 25 AIS channels; the mean and standard deviation of each of the 25 distributions are calculated by fitting the matrix $\mathbf{H}$ to lognormal distributions, but not supplanting it.

       If we let the lognormal probability distribution function be $\widehat{\Omega}_i$, then the full calculated distribution is $\Omega = \sum_{i=1}^{25} \phi_i \widehat{\Omega}_i$,

225   where ϕ_i are the elements of $\boldsymbol{\phi}$; and Ω is the calculated total charged (negative or positive, $\Omega_\pm$) distribution. We minimize the residuals between the calculated current (I_{calc}) and the measured current (I_{meas}) from AIS using nonlinear least squares, with 25 concentration coefficients as free parameters. We solve the nonlinear least squares computationally and we do not supplement it with any regularization technique. The procedure is repeated for each polarity separately, hence the resulting distributions are $\Omega_\pm$. (More details are provided in Sect. 4 by Mirme and Mirme (2013) on the theoretical basis for $\mathbf{H}$.)

230   A known limitation of the AIS is its inability to detect ions whose mobility diameter is lower than 0.82 nm (Manninen et al., 2016). To this end, we extrapolate the missing measurements by assuming the ion distribution follows a lognormal distribution even below 0.82 nm. This extension allows us to account for a wider distribution of available ions, especially where the expected value of collisions is higher (smaller ions collide at a higher rate with the same reference oppositely charged particle).

235   While we find our approach to be more useful with multiply charged particles than the standard procedure, it does not deviate significantly from the standard procedure by Mirme and Mirme (2013) under normal operating conditions. Compared to five randomly selected nucleation experiments conducted throughout the same CLOUD campaign, where no

significant multiply charged particles are expected, we find a median of about 12 % deviation (over all mobilities) between our modified method and the original method.

2.2.2 Multi-charge inference

When operated in "Ion Mode" like in our case, the typical AIS inversion provides information directly only about singly charged particles (Manninen et al., 2016). However, we are interested in multiply charged particles which are briefly present away from steady state. To deduce information about multiply charged particles present in our experiments from the total charged distributions from Sect 2.2.1 ($\Omega_\pm$), we identify a time when the steady-state assumptions are expected to hold: We postulate this happens at the end of the decay stage when the ratio of the positive and negative concentrations tends to be unity. Once in steady state after interacting with ions produced from GCR, it is reasonable to assume that all multiply charged particles have been neutralized due to collisions with ions of opposite polarity.

At the end of the decay stage, $t = t_{\mathrm{end}}$, we set the concentration of singly charged positive particles to be the same as the inferred concentration from the AIS in Sect. 2.2.1; that is, as $\Omega_+(d_\mathrm{p};\ t = t_{\mathrm{end}}) = \Omega_-(d_\mathrm{p};\ t = t_{\mathrm{end}})$, we assume all of particles in $\Omega_+(d_\mathrm{p};\ t = t_{\mathrm{end}})$ are singly (positively) charged. Our goal is to then estimate $\Omega_+(d_\mathrm{p};\ t < t_{end})$ as a combination of multiply charged distributions as in Eq. (1), where γ_j are free parameters that determine the total number of particles of a given charge state j and $\hat\omega$ is the density function for each charging state. We further assume the dynamic evolution of $\Omega_+(d_\mathrm{p};\ t)$ can be described as a first-order loss process (to walls and dilution) as the charges themselves are simply redistributed among charging states. For ease of presentation, we set $\omega_j = \gamma_j\ \hat\omega_j$ after this section.

$$\Omega_+(t) = \sum_{j=1}^{911} \gamma_j\, \hat\omega_j = \sum_{j=1}^{911} \omega_j \tag{1}$$

We assume the probability density function $\hat\omega_1$ has the same shape as $\Omega_+(d_\mathrm{p};\ t = t_{\mathrm{end}})$ as in Eq. (2) after accounting for wall, dilution, and coagulation losses. While coagulation can play a role in the shape of the distribution $\hat\omega_1$, wall loss and dilution loss are clearly dominant in our experiments (see Figure 2).

$$\hat\omega_1 = \frac{\Omega_+(d_\mathrm{p};\ t_{\mathrm{end}})}{\int_0^\infty \Omega_+(d_\mathrm{p};\ t_{\mathrm{end}})\ \mathrm{d}\ln d_\mathrm{p}} \tag{2}$$

At the end of the decay stage, $\gamma_1 = \int_0^\infty \Omega_+(d_\mathrm{p};\ t_{\mathrm{end}})\ \mathrm{d}\ln d_\mathrm{p}$ and $\gamma_{j\neq1} = 0$ by definition. Since $\hat\omega_1$ is now known, we can estimate $\hat\omega_j$ using the Millikan equation relating electric mobility, charge number, and particle diameter (Lehtinen and Kulmala, 2003; Mirme and Mirme, 2013; Manninen et al., 2016). For the same electric mobility Z_p, different pairs of charge number j and particle diameter d_p are linked through Eq. (3) assuming constant viscosity η and elementary charge constant q (C_c is the Cunningham's slip correction factor which depends on size). We use Eq. (3) to estimate $\hat\omega_j$ by shifting $\hat\omega_1$ in diameter, holding everything else constant.

$$Z_p = \frac{j\, q\, C_c(d_p)}{3\,\pi\,\eta\,d_p}$$

(3)

We finally add one correction to ω_j. As the AIS uses the electric mobility diameter, multiply charged particles will be detected at higher mobilities than their singly charged counterparts. And since they carry more charges, the measured current will be higher. Thus, we divide each ω_j by its charge state j and we use the mobility diameter throughout our calculations as retrieved by Eq. (3). All in all, ω_j can be expressed as in Eq. (4) as a size- and time-dependent function of γ_j, the positive charge concentration Ω_+, and a loss constant k_{loss} related to particle losses wall, dilution, and coagulation).

270
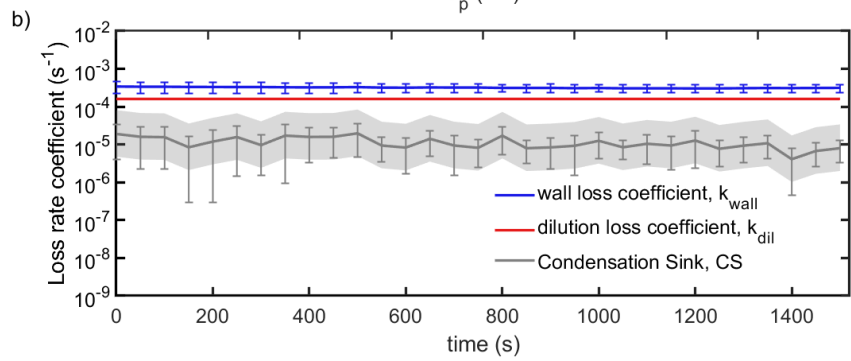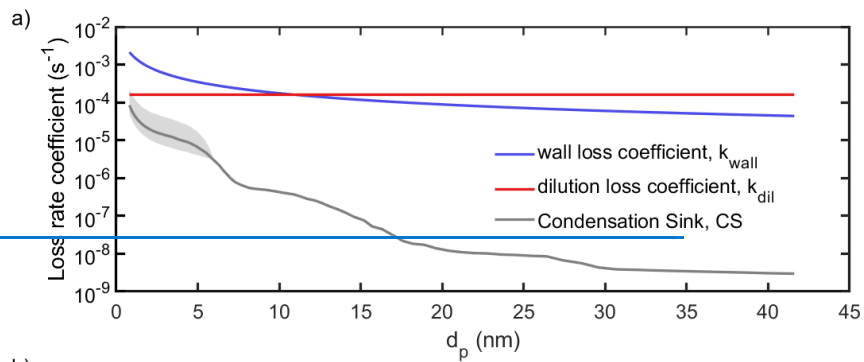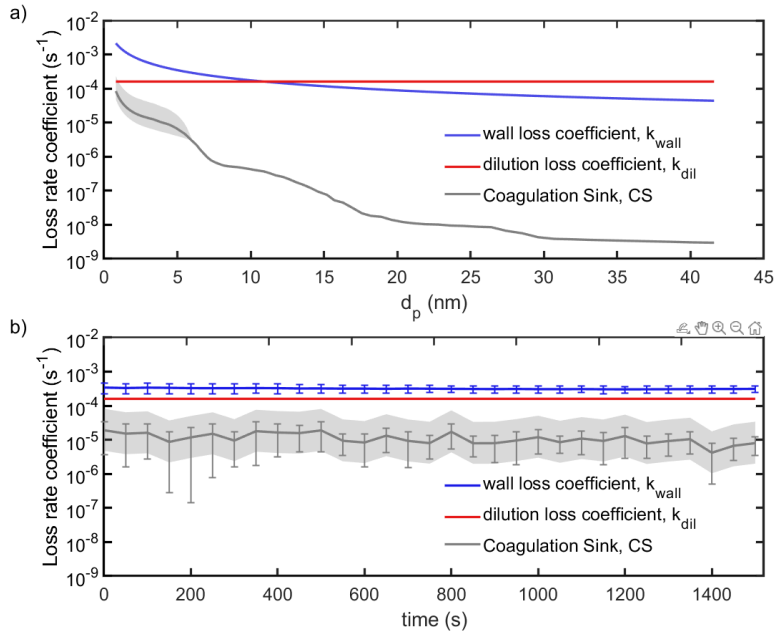
Figure 2: Summary of the particle loss rates during the decay stage. a) Size dependency of the loss rates for a distribution (ω_j) during a decay stage (averaged over an entire decay period). b) The loss rates due to different processes for a given distribution ω_j as a function of time during a decay stage. The grey bands indicate uncertainty ranges resulting from errors on measurements of the total particle number concentrations below 6 nm. We assume generous ($\pm$ 400 %) errors since instruments can vary widely at small particle sizes (Kangasluoma

275 et al., 2020).

$$\omega_j(t) = \frac{\gamma_j}{\sum_{j=1}^{11}\gamma_j}\,\Omega_+\big(d_\mathrm{p};\,t\big)\,e^{-k_\mathrm{loss}t} \qquad (4)$$

We note that in estimating ω_j in Eq. (4), we assume measurements below 2 nm electric mobility diameter are singly charged or neutral as most entities present below 2 nm can be safely considered ions whose concentration is accounted for in $\Omega_\pm$ from, Sect 2.2.1. Moreover, we simplify our calculation by assuming all measurements above 10 nm electric mobility diameter to

280 be at most singly charged as well. We are able to make these two assumptions because the CHARGE instrument produces particles of sizes around 6 nm electric mobility diameter. Consequently, the total number concentration decreases significantly above 10 nm and below 2 nm, and so does the ratio of multiply charged particles in it as well, and the timescale of neutralization (i.e., timescale to ~~reach~~ reaching particle charge steady state) for particles bigger than 10 nm is significantly faster than for

smaller ones. While the limits of this interval are arbitrary, their values are allowed to vary within a range of ± 50 % in the error estimation calculation as discussed in the Supplementary Information.

2.2.3 Population balance

We derive the ion–aerosol rate coefficients from data collected during the decay stage. Since the CHARGE instrument produces and injects particles at high flow rate (200 l min^{-1}), the flow rates in the CLOUD chamber are not balanced immediately after an injection stage. Thus, the decay stage starts as soon as the flow inside the chamber is in steady state, which can be estimated from the flow rates exiting the chamber and from the overpressure inside the CLOUD chamber. We account for the production and loss terms of all the particles and ions inside the chamber as a function of time. After injection, particles and ions in the chamber dynamically evolve in time due to several processes, related to chamber dilution, wall processes, aerosol–aerosol collisions, and ion–aerosol collisions. The individual loss rates and their time dependence during our experiments are summarized in Figure 2.

In the CLOUD chamber during these experiments, the dilution rate coefficient, k_{dil}, was constant at 1.60×10^{-4} s^{-1}, which is the result from dividing the volume flow rate (250 l min^{-1}) by the total volume (26.1 m^3) (e.g., Simon et al., 2016; Pfeifer et al., 2020). The chamber wall loss rate coefficient is calculated using $k_{wall} = C_{wall} \sqrt{D_p}$, where D_p is the particle diffusion coefficient and C_{wall} is a proportionality constant whose value has been measured as 7.70×10^{-3} cm^{-1} s$^{-1/2}$ based on wall loss of sulfuric acid vapour (Metzger et al., 2010; Ehrhart et al., 2016; Stolzenburg et al., 2020; He et al., 2021). For the collisions involving at least one neutral aerosol particle, we follow Seinfeld and Pandis (2016) to estimate the coagulation rate coefficient, K, between neutral particles and thus the coagulation sink, CS. We account for the effects of charges on coagulation in the calculation of β in the following paragraphs.

The main goal of our experiment is to quantify the ion–charged aerosol rate coefficients, which play a role in the dynamic evolution of the particle size distribution and particle charge distribution. More precisely, we estimate the rate coefficients, $\beta_j = \beta_{-,j}$, between the negative ion distribution (< 2 nm) and the particle distribution (2–10 nm) with j positive charges. By setting up the balance equations, we track the number and charge evolution over time and thus constrain $\beta_j(d_p)$.

Beyond these terms, we assume sources and sinks related to evaporation, condensation, and nucleation are negligible in our experiments. At 80 % relative humidity and 278 K, the evaporation of sulfuric acid is negligible (Stolzenburg et al., 2020). We assume the growth rates of particles in our experiment are on the order of 1.8 nm hour^{-1} as those reported for sulfuric acid–water systems (Nieminen et al., 2010). These growth rates are too small to influence the dynamics herein, especially compared with the duration of the experiments (at most 1500 s). Using parameterizations for the sulfuric acid-water system from Vehkamäki et al. (2002), we calculate nucleation rates of about 2.5×10^{-8} cm^{-3} s^{-1} for the measured sulfuric acid concentrations (about 5×10^7 cm^{-3} in the beginning of a decay and during injection), which is negligible (Vehkamäki et al., 2002; Dunne et al., 2016). We assume particles produced inside the chamber during the experiments consist of sulfuric acid and water with a uniform density of 1600 kg m^{-3} (Myhre et al., 1998). (The robustness of these assumptions is verified in the

Supplementary Information, where we randomly vary all parameters. For example, the density is varied between that of pure water (997 kg/m3) and that of pure sulfuric acid (1830 kg/m3), finding negligible sensitivity of the assumption herein.)

From Sect 2.2.2, using AIS measurements, we obtain $\Omega_\pm$ as a distribution over sizes 0.2–40 nm of diameters and ω_j as a distribution over sizes 2–40 nm of diameters. We also infer Ω_0, which is the distribution of neutral entities over sizes 2–40 nm of diameters by combining AIS and nSMPS measurements. We can thus write the balance equations for the positively charged particles compactly in Eq. (6), which is valid for $1 < j < 9\text{11}$. However, because of the size dependence of Ω and ω, we introduce a coefficient σ to account for the size dependency normalized by its value at the lowest size (ion size). That is, σ is unity at the ion size (1 nm diameter) and it is less than unity for bigger sizes. This formulation yields β for the ion–aerosol coefficients while still accounting for events including charged particles and ions in the rest of distribution that are ignored earlier in using K. We use the Coulombic enhancement coefficient to calculate σ following Seinfeld and Pandis (2016; p. 564, Eq. 13A.16), with d_{p1} and d_{p2} referring to the sizes of coagulating particles in nm in Eq. (5).

$$\breve{\sigma}_j(d_{p1}, d_{p2}) = -\frac{j}{d_{p1} + d_{p2}} \frac{1}{\exp\left(-\frac{j}{d_{p1} + d_{p2}}\right) - 1}; \quad \sigma_j = \frac{\breve{\sigma}_j(d_{p1}, d_{p2})}{\breve{\sigma}_j(d_{p1} = 1\,\text{nm}, d_{p2})} \tag{5}$$

$$\frac{d\omega_j}{dt} = \sigma_{j+1}\,\beta_{j+1}\,\Omega_-\,\omega_{j+1} - \sigma_j\,\beta_j\,\Omega_-\,\omega_j - L_j \tag{6}$$

In Eq. (6), the positively charged size distribution ω at each charge state j evolves in time due to production and loss. On the right-hand side, the first term denotes the gain of a particle of charge j as a result of a coagulation event between a particle of charge $j + 1$ of concentration ω_{j+1} and a negative ion of concentration Ω_-. The second term denotes the loss of a particle of charge j and of concentration ω_j as it collides with a negative ion of concentration Ω_-. The third term lumps all other losses, which are to the wall, dilution, and coagulation sink (CS; including in-distribution losses, that is, coagulation within the distribution of particles of diameters 2–10 nm) as shown in Eq. (7).

$$L_j = \omega_j(k_{\text{wall}} + k_{\text{dil}} + \text{CS}) = \omega_j(k_{\text{wall}} + k_{\text{dil}}) + \omega_j \sum_l K_l\,\omega_l \tag{7}$$

To complete the description in Eq. (6), we use Eq. (8) and Eq. (9) for the cases $j = 1$ and $j = 9\text{11}$, respectively. In Eq. (8), we use β_0 to denote collision coefficient between positive small ions Ω_+ ($d_p < 2\text{nm}$) and neutral particles Ω_0 inferred from the NAIS and nSMPS measurements. As such, β_0 is calculated in the same way K_l in Eq. (7) is calculated, following Seinfeld and Pandis (2016).

$$j = 1; \qquad \frac{d\omega_j}{dt} = \beta_0\,\Omega_+\,\Omega_0 + \sigma_{j+1}\beta_{j+1}\,\Omega_-\,\omega_{j+1} - \sigma_j\beta_j\,\Omega_-\,\omega_j - L_j$$
$$= K\,\Omega_+\,\Omega_0 + \sigma_{j+1}\beta_{j+1}\,\Omega_-\,\omega_{j+1} - \sigma_j\beta_j\,\Omega_-\,\omega_j - L_j \tag{8}$$

$$j = 9\text{11}; \qquad \frac{d\omega_j}{dt} = -\beta_j\Omega_-\omega_j - L_j \tag{9}$$

The system of equations (Eq. 6, 7, and 8) is solved numerically for each time step during the decay stage. One time step corresponds to the duty cycle of the AIS (50 s) and the nSMPS measurement is synchronized to this time step using linear interpolation. Accordingly, for each charge number j, there exists one solution for each cycle of 50 s, where the calculation is only solved within the respective lifetime of each ω_i. The lifetime is determined using an exponential fit through the time evolution of each ω_i. For example, $j = 9$ with an estimated lifetime of 200 s yields four measurements (one each 50 s) and thus four coefficients are calculated for this charge number in this specific experiment. For smaller j, the lifetime increases and thus, more coefficients are calculated per experiment.
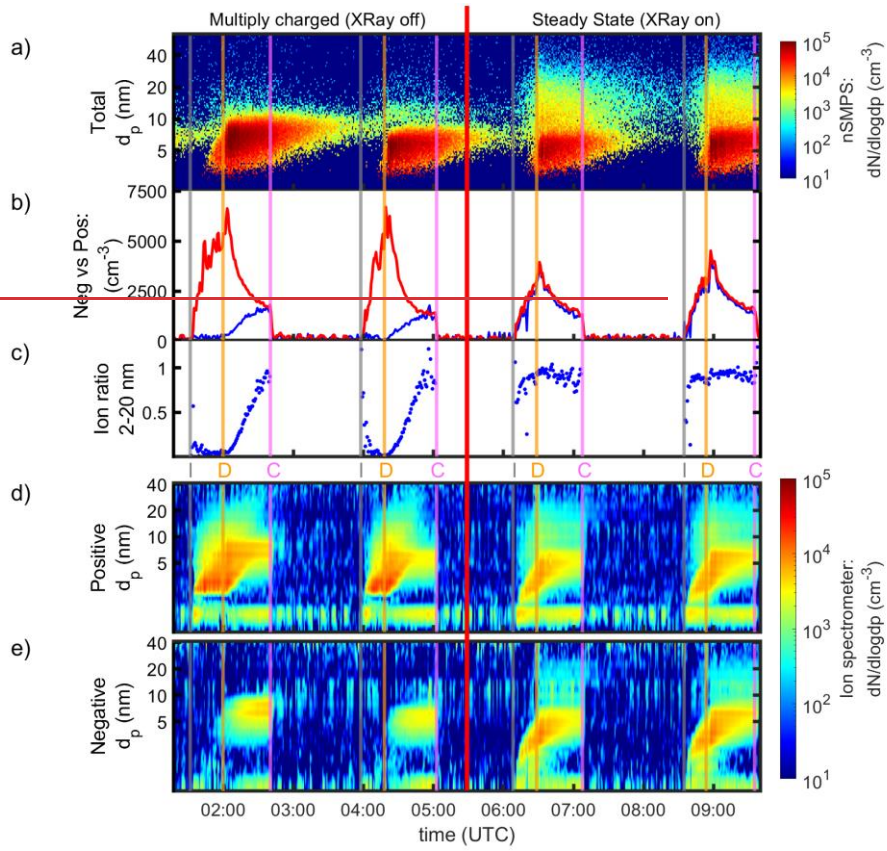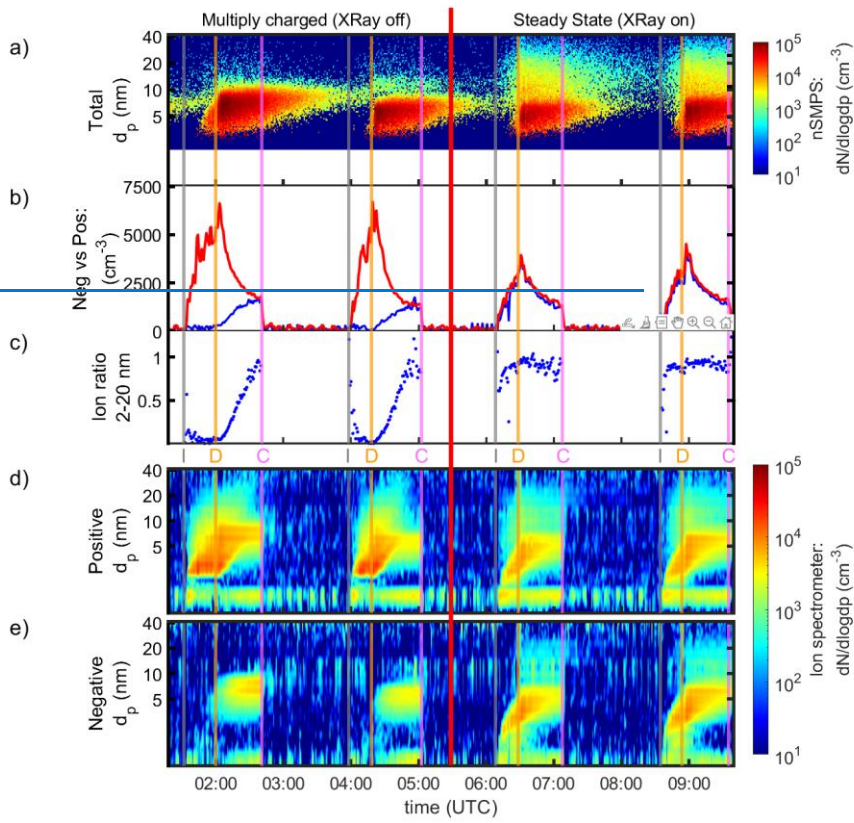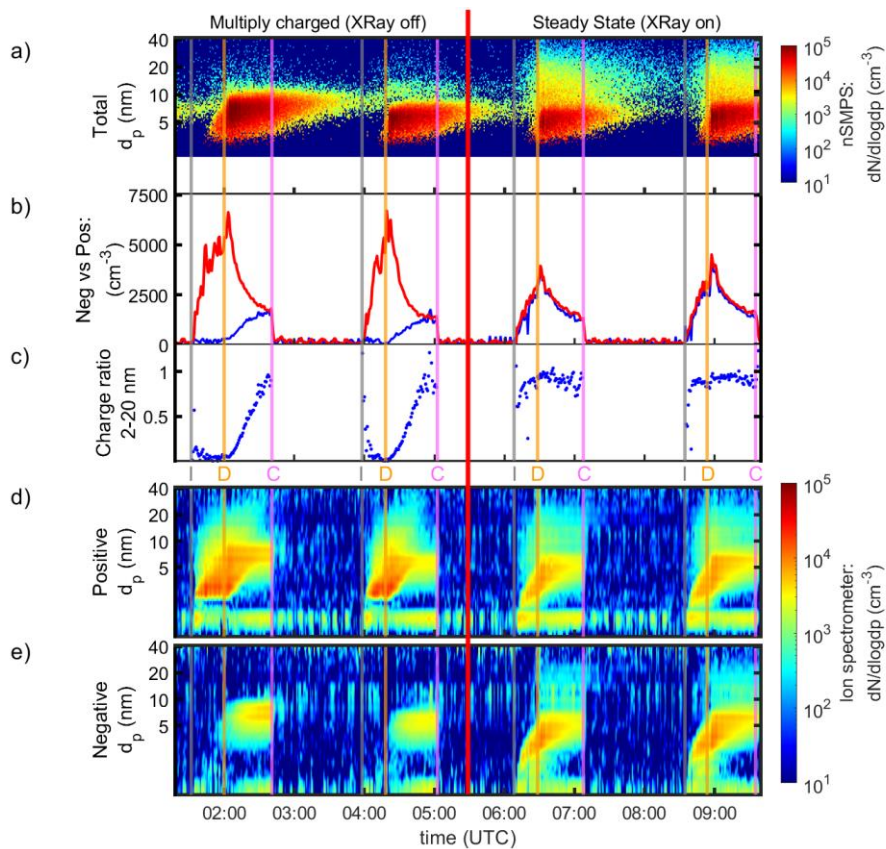
Figure 3: Example experiments performed without and with charge neutralisation by X-rays. Time series showing two experiments
with X-ray off followed by two experiments with X-ray on (separated by the red vertical line). The grey vertical line marks the beginning of
an injection stage (I), the orange line a decay stage (D) and the pink line a cleaning stage (C). The panels show the time series of a) particle
size distributions measured with a nSMPS, b) number concentrations of positive (red) and negative (blue) charged particles, c)
negative:positive charged particle ratio, and d) positive and e) negative charged particle apparent size distributions measured with an AIS.
Here the apparent size incorrectly assumes singly charged particles.

 3. Results

In Figure 3, we show a time series of two experiments with X-ray off and two with X-ray on. A total of four experiments without X-ray and two with X-ray were conducted to ensure reproducible results. As detailed in Sect. 2.1, particle measurements were carried out with an NAIS (Manninen et al., 2016, 2009) and an SMPS (Tritscher et al., 2013) for the total particle concentration. Gas phase concentrations were measured using several mass spectrometers (Kürten et al., 2011, 2012; Breitenlechner et al., 2017; Wang et al., 2021). We calculate the ion–aerosol rate coefficients during the decay stage starting as soon as the chamber flow is in steady state after injection. We note that the negative and position ion distributions in panel b approach are similar to the canonical value of 1500 cm^{-3} often reported for ion concentrations in the atmosphere. More precisely, the concentration of positive ions averages around 1500 cm^{-3} while the negative ions around 1350 cm^{-3}, agreeing with previous studies showing the concentration of negative ions is often lower (Franchin et al. 2015).

With the X-ray off, we observe almost no negative ions during injection. Negative ions are entirely consumed by ion–ion recombination and ion–aerosol attachment as there is a significant amount of positive charge available during injection via the positively charged particles formed. However, we observe an increase in the number of negative ions during the decay stage, which can only come from ion–aerosol attachment of (singly charged) negative ions with (neutral) particles.

With the X-ray on, we observe that the ratio between positively to negatively charged particles is almost unity. This indicates that the X-ray source effectively pushes a large fraction of particles to its steady state particle charge distribution. Thus, it seems natural that we can assume that all particles carry at most $j = 1$ charges during experiments with the X-ray on. However, when assuming charge steady state with maximum $j = 1$ charge, our calculations result in systematically smaller coefficients during the experiments with the X-ray on compared to the experiments with the X-ray off. This implies that there is an additional source term in the case of experiments with the X-ray on. Since the particles from the CHARGE Electrospray Generator pass the X-ray source at a flow rate of 200 l lpmin^{-1}, it is plausible to assume that a few particles are still doubly charged in the beginning of the decay stages. For these experiments, we therefore calculate rate coefficients twice: once assuming charge steady state (maximum $j = 1$ charges) and once including a small fraction of doubly charged particles, that is, (assuming singly:doubly charged ratio of 5:1 at the beginning of the decay stage). The latter assumption is further justified by the presence of the seemingly larger particles in the steady-state cases; the nSMPS inversion algorithm assumes at most singly charged particles after passing the particles through the nSMPS's neutralizer, and compensates for this seemingly erroneous assumption by counting multiply charged particles as larger particles. We show the charge fraction of positively charged particles in the first experiment in Figure 3 in the Figure S4 in the SI.

The total distribution is similar in both experiments in Figure 3 and observed deviations in the size distributions between NAIS and nSMPS are within the expected range from other measurements (Kangasluoma et al., 2020). During both experiments, as expected, a significant fraction of the particle distribution is neutral (approximately 98 %). SMPS measurements are subject to measurement errors especially below 6 nm (Kangasluoma et al., 2020); however, during our experiments, the influence of the measured total particle concentration on the calculation of the rate coefficients is relatively

small, since wall loss and dilution loss dominate (see Figure 2). Further, the influence of varying the concentrations measured by the SMPS within the estimated error range is also discussed in the Supplementary Information and shown in Figure S3.

390   Figure 4 summarizes the calculated rate coefficients from our experiments. The error bars indicate the one-sigma confidence interval of numerical solutions from all experiments (for all time steps) for the respective charge number j. The calculations are carried out for maximum $j = 11$ charges, with the assumptions summarized in Sect. 2. To calculate the "best fit" values from all our data, we use an exponential fit through the respective experiments, which is solved using nonlinear least squares. It is based on the same production and loss rates as in case of the numerical solution in Sect. 2.2.3. In contrast to

395 the numerical solution, steady state conditions are assumed in the case of this fit, except for ion–aerosol collisions. As such, we take time-averaged values for various coefficients in Eq. (10). As an example, for $j = 1$ charge, the approximation by the fit is described following Eq. (8) by Eq. (10) below.

$$\omega_j(t) = \omega_{j,t=0} \exp\left(-\left(\overline{k_{wall} + k_{dil} + CS} - \frac{\overline{\beta_0 \, \Omega_+ \, \Omega_0}}{\overline{\Omega_+}} + \beta_j \sigma_i \Omega_- - \frac{\beta_{j+1} \sigma_{j+1} \Omega_- \, \omega_{j+1}}{\omega_j}\right) + \omega_{j,\infty}\right) \tag{10}$$

In Eq. (10), $\omega_{j,\infty}$ denotes instrumental background at the end of the decay stage and $\omega_{j,t=0}$ is the concentration at the beginning of the decay stage. The best fit of the numerical solution and the one-sigma confidence interval are summarized in Table 1. In

400 Figure 4, we compare our measurements with leading representative models and with the MD simulations from Tamadate et al. (2020b). Our results confirm the robustness of the selected models calculating the ion–aerosol rate coefficient (López-Yglesias and Flagan, 2013; Gopalakrishnan and Hogan, 2012; Gatti and Kortshagen, 2008; D'yachkov et al., 2007), which we calculate using the particula software package, version 0.0.10 (Mahfouz et al., 2022). In particular, we find the results by Gatti and Kortshagen (2008) and López-Yglesias and Flagan (2013) to be most compatible with our experimental estimation.
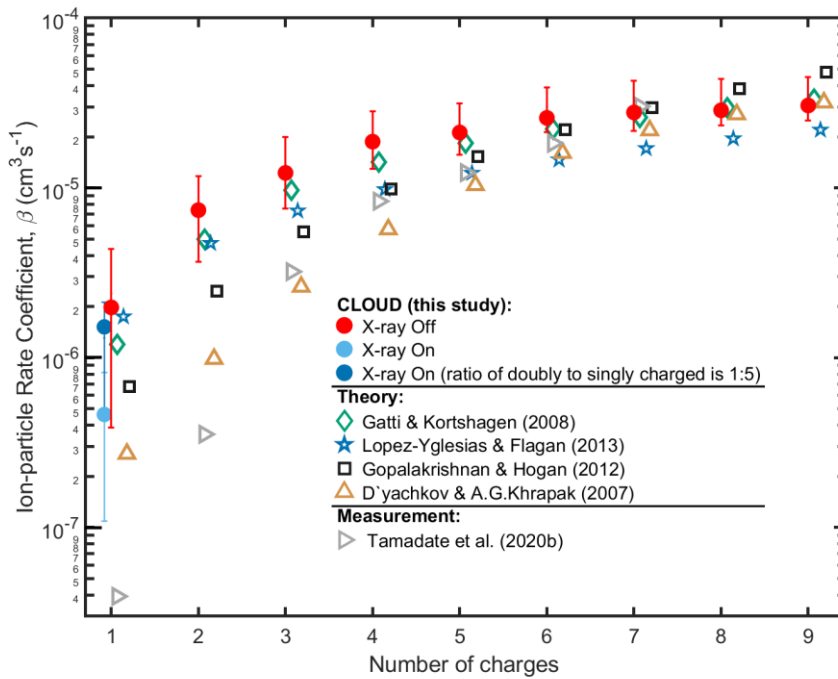
405

Figure 4: Ion–particle rate coefficients versus number of charges on the particle. The CLOUD measurements are indicated by filled circles that are coloured red for X-ray off experiments, blue for X-ray on experiments assuming full steady state ion distributions, and cyan for X-ray on and assuming incomplete steady state ion distributions. Theoretical predictions based on the limiting-sphere paradigm and Langevin dynamics are shown in open symbols for 1 nm negative ions colliding with positively charged particles of 6 nm diameter. Recent
410 results for multiply charged PEG$_{4600}$ particles with ions are shown in grey triangles (Tamadate et al., 2020b). The symbols are offset from integer charges to improve their visibility.

Table 2. Experimentally inferred ion–aerosol rate coefficients.

Number of charges j	Best fit β_j (cm^{3}s^{-1}) $\times 10^{-6}$	One-sigma confidence interval $\times 10^{-6}$
1	2.0	[0.4, 4.4]
(1) (X-ray on)	1.5	[0.1, 2.1]

2	7.4	[3.7, 11.7]
3	12.2	[7.5, 19.9]
4	18.7	[13.0, 28.2]
5	21.2	[15.6, 31.5]
6	25.8	[21.2, 39.0]
7	27.8	[21.7, 42.8]
8	28.6	[23.4, 44.0]
9	30.6	[24.9, 45.1]

4. Discussion

In general, we find the limiting-sphere model by López-Yglesias and Flagan (2013) and linear combination of models by Gatti and Kortshagen (2008) to best represent our experimentally determined rate coefficients. It is imperative to note that while the approach based on the limiting-sphere is fine-tuned to atmospheric applications (meaning parameterized for atmospheric ions and conditions), the approaches based on mean first-time passage and dimensional analysis (e.g., ones by Gopalakrishnan and Hogan (2012) and others following it) are more general. This could explain the discrepancy — in other words, adjusting the input parameters of the latter approach could lead to a better fit with our data. Notwithstanding this discrepancy, the results from all theoretical models point to similar trajectory. ~~Remarkably, our~~ Our results most resemble the analytical model by Gatti and Kortshagen (2008) as reformulated by Gopalakrishnan and Hogan (2012). In their model, a linear combination of continuum, free molecular, and transition regimes is used to describe collisions of nanoparticles in plasmas.

We compare our results to recent results based on continuum–MD simulations (Tamadate et al., 2020b), which are for multiply charged PEG_{4600} particles with ions. ~~O~~While ~~o~~ur results align well with previous models (López-Yglesias and Flagan, 2013; Gopalakrishnan and Hogan, 2012; Gatti and Kortshagen, 2008; D'yachkov et al., 2007).~~,~~ Additionally, ~~we find our results deviate from those by Tamadate et al. (2020b) especially for a low number of charges (<5). This could be explained by the geometry (and thus size) of the simulated PEG₄₆₀₀ particles.~~ ~~We note that~~ our results align with all models, including the additional one by Tamadate et al. (2020b), for >5 charges where the effect of charge likely outweigh the effects of geometry. Nonetheless, we find our results deviate from those by Tamadate et al. (2020b) especially for a low number of charges (<5). This could be explained by the geometry (and thus size) of the simulated PEG_{4600} particles. Moreover, the flexible nature of the ions and particles in their study likely plays a central role and cannot be compared directly to our results herein.

The primary implication of our results here is providing an experimental basis for model calculations of the ion–aerosol rate coefficient. In so doing, this enables researchers to implement and tune model calculations more readily like those based on the limiting-sphere or Langevin dynamics approaches cited earlier. This eventually provides further evidence in constraining the cosmic galactic rays' role in climate change. While availability of ions generated by cosmic rays can influence

new-particle formation and growth to an extent, their influence is dampened by the fact that charged particles are more readily scavenged by existing bigger particles (Mahfouz and Donahue, 2021a). In the limit, this scavenging rate is doubled, and the

440 probability of survival is thus squared (Mahfouz and Donahue, 2021a, b). However, questions remain open regarding ion–aerosol interactions in scenarios close to aerosol–cloud interactions and the subsequent interactions between ions and climate variability (e.g., Guo and Xue, 2021; Tinsley, 2022). Furthermore, the comparison with the results by Tamadate et al. (2020b) shows that future studies will need to focus on the dependency of parameters kept constant in this study, for example, relative humidity, chemical composition, and turbulence. This experimental procedure will enable further exploration and experimental

445 evidence in resolving these questions, e.g., in designing and building experiments in cloud chambers.

~~With this first set of novel experiments, we have successfully constrained the coagulation rate coefficients between negative atmospheric ions and positively charged particle distributions in the size range 2–10 nm for up to nine charges. Using the same experimental framework, we additionally can study interactions between atmospheric ions and neutral particles, where induced charges can potentially impact the rate coefficient and thus alter the ensuing particle dynamics. Together, these~~

450 ~~efforts will not only illuminate any effect of galactic cosmic rays on climate change, but also the effect of extreme conditions — where excess of charges and ions are readily available — on particle formation and growth, subsequent aerosol dynamics, and eventually weather and climate phenomena.~~

5. Summary

In this study, we present novel experiments to calculate ion–aerosol rate coefficients under atmospherically relevant conditions

455 in the CERN CLOUD chamber. After assessing the robustness of our calculations, we test our experimentally inferred results against those predicted by leading models. We find overall agreement with the selected models, but especially with one employing a linear combination of limiting behaviours across regimes (Gatti and Kortshagen, 2008). This study, and follow-up experiments, will help constrain charge-related dynamics affecting atmospheric particles, which can play an important role in the formation and growth of particles as well as the subsequent dynamics in thunderstorm and non-thunderstorm clouds.

460

Data availability. All data used in this study, including the codes, are available at DOI: 10.5281/zenodo.7335017. The **H** matrix used in this study is provided with permission (Mirme and Mirme, 2013) as part of the data linked.

Author contributions. JP, SM, HEM and JK developed the CHARGE electrospray generator. JP, NGAM, BS, SM, RB, ZB,
465 LC, LD, MG, XH, BL, VM, RM, BM, AO, MP, AAP, BR, MS, PT, NSU, DSW, MW, SKW, AW, MZW, WY, IEH, KL, MK, TP, AT, SM, HEM, and JK prepared the CLOUD facility and measurement instruments. JP, NGAM, BS, LC, LD, MG, XH, HL, RM, BM, TM, AAP, BR, DSW, SKW, AW, MZW, AA, AT, SM, HEM, AK, and JK collected the data. JP, NGAM, BS and DS analysed the data. JP, NGAM, BS, SM, DS, LD, XH, SKW, AW, IEH, NMD, RCF, AK, JC and JK contributed to the scientific discussion. JP, NGAM, DS, NMD, RCF, AK and JK contributed to writing the manuscript.

470

Competing interests. The authors have the following competing interests: At least one of the (co-)authors is a member of the editorial board of Atmospheric Chemistry and Physics.

Acknowledgements. We thank CERN for supporting CLOUD with technical and financial resources. We thank Louis-Philippe De Menezes, Ilia Krasin, Xavier Pons, and Robert Kristic for their contributions to the experiment. This research was performed before the invasion of Ukraine by Russia on 24 February 2022.

Financial support. This research has been supported by Innovative Training Networks – ITN 400 (CLOUD-Motion H2020-MSCA-ITN-2017 no. 764991), the German Ministry of Science and Education (CLOUD-16, 01LK1601A), the European Union's Horizon 2020 research and innovation programme under the Marie Sklodowska-Curie grant agreement no. 764991 ("CLOUD-MOTION H2020-MSCA-ITN2017"), the Swiss National Science Foundation (grant numbers 200021_169090, 200020_172602 and 20FI20_172622), European Union's Horizon 2020 research and innovation programme under the Marie Sklodowska-Curie grant agreement no. 895875 ("NPF-PANDA"), ACCC Flagship funded by the Academy of Finland grant number 337549, Academy professorship funded by the Academy of Finland (grant no. 302958), Academy of Finland projects no. 325656, 316114, 314798, 325647, 341349 and 349659. "Quantifying carbon sink, CarbonSink+ and their interaction with air quality" INAR project funded by Jane and Aatos Erkko Foundation, Jenny and Antti Wihuri Foundation project "Air pollution cocktail in Gigacity", European Research Council (ERC) project ATM-GTP Contract No. 742206, and the Arena for the gap analysis of the existing Arctic Science Co-Operations (AASCO) funded by Prince Albert Foundation Contract No 2859, FCT-Portuguese national funding agency for science, research and technology, project CERN/FIS-COM/0028/2019.

Review statement.

References

Amanatidis, S., Huang, Y., Pushpawela, B., Schulze, B. C., Kenseth, C. M., Ward, R. X., Seinfeld, J. H., Hering, S. V., and Flagan, R. C.: Efficacy of a portable, moderate-resolution, fast-scanning differential mobility analyzer for ambient aerosol size distribution measurements, Atmos. Meas. Tech., 14, 4507–4516, https://doi.org/10.5194/amt-14-4507-2021, 2021.

Birmili, W., Stratmann, F., Wiedensohler, A., Covert, D., Russell, L. M., and Berg, O.: Determination of Differential Mobility Analyzer Transfer Functions Using Identical Instruments in Series, Aerosol Science and Technology, 27, 215–223, https://doi.org/10.1080/02786829708965468, 1997.

Breitenlechner, M., Fischer, L., Hainer, M., Heinritzi, M., Curtius, J., and Hansel, A.: PTR3: An Instrument for Studying the Lifecycle of Reactive Organic Carbon in the Atmosphere, Anal. Chem., 89, 5824–5831, https://doi.org/10.1021/acs.analchem.6b05110, 2017.

Chahl, H. S. and Gopalakrishnan, R.: High potential, near free molecular regime Coulombic collisions in aerosols and dusty plasmas, Aerosol Science and Technology, 53, 933–957, https://doi.org/10.1080/02786826.2019.1614522, 2019.

Dada, L., Lehtipalo, K., Kontkanen, J., Nieminen, T., Baalbaki, R., Ahonen, L., Duplissy, J., Yan, C., Chu, B., Petäjä, T., Lehtinen, K., Kerminen, V.-M., Kulmala, M., and Kangasluoma, J.: Formation and growth of sub-3-nm aerosol particles in experimental chambers, Nat Protoc, 15, 1013–1040, https://doi.org/10.1038/s41596-019-0274-z, 2020.

Dépée, A., Lemaitre, P., Gelain, T., Monier, M., and Flossmann, A.: Laboratory study of the collection efficiency of submicron aerosol particles by cloud droplets – Part II: Influence of electric charges, Atmos. Chem. Phys., 21, 6963–6984, https://doi.org/10.5194/acp-21-6963-2021, 2021.

Dias, A., Ehrhart, S., Vogel, A., Williamson, C., Almeida, J., Kirkby, J., Mathot, S., Mumford, S., and Onnela, A.: Temperature uniformity in the CERN CLOUD chamber, Atmos. Meas. Tech., 10, 5075–5088, https://doi.org/10.5194/amt-10-5075-2017, 2017.

Dunne, E. M., Gordon, H., Kürten, A., Almeida, J., Duplissy, J., Williamson, C., Ortega, I. K., Pringle, K. J., Adamov, A., Baltensperger, U., Barmet, P., Benduhn, F., Bianchi, F., Breitenlechner, M., Clarke, A., Curtius, J., Dommen, J., Donahue, N. M., Ehrhart, S., Flagan, R. C., Franchin, A., Guida, R., Hakala, J., Hansel, A., Heinritzi, M., Jokinen, T., Kangasluoma, J., Kirkby, J., Kulmala, M., Kupc, A., Lawler, M. J., Lehtipalo, K., Makhmutov, V., Mann, G., Mathot, S., Merikanto, J., Miettinen, P., Nenes, A., Onnela, A., Rap, A., Reddington, C. L. S., Riccobono, F., Richards, N. A. D., Rissanen, M. P., Rondo, L., Sarnela, N., Schobesberger, S., Sengupta, K., Simon, M., Sipilä, M., Smith, J. N., Stozhkov, Y., Tomé, A., Tröstl, J., Wagner, P. E., Wimmer, D., Winkler, P. M., Worsnop, D. R., and Carslaw, K. S.: Global atmospheric particle formation from CERN CLOUD measurements, Science, 354, 1119–1124, https://doi.org/10.1126/science.aaf2649, 2016.

D'yachkov, L. G., Khrapak, A. G., Khrapak, S. A., and Morfill, G. E.: Model of grain charging in collisional plasmas accounting for collisionless layer, Physics of Plasmas, 14, 042102, https://doi.org/10.1063/1.2713719, 2007.

Ehrhart, S., Ickes, L., Almeida, J., Amorim, A., Barmet, P., Bianchi, F., Dommen, J., Dunne, E. M., Duplissy, J., Franchin, A., Kangasluoma, J., Kirkby, J., Kürten, A., Kupc, A., Lehtipalo, K., Nieminen, T., Riccobono, F., Rondo, L., Schobesberger, S., Steiner, G., Tomé, A., Wimmer, D., Baltensperger, U., Wagner, P. E., and Curtius, J.: Comparison of the SAWNUC model with CLOUD measurements of sulphuric acid-water nucleation, J. Geophys. Res. Atmos., 121, 401-412, https://doi.org/10.1002/2015JD023723, 2016.

Flagan, R. C.: History of Electrical Aerosol Measurements, Aerosol Science and Technology, 28, 301–380, https://doi.org/10.1080/02786829808965530, 1998.

Franchin, A., Ehrhart, S., Leppä, J., Nieminen, T., Gagné, S., Schobesberger, S., Wimmer, D., Duplissy, J., Riccobono, F., Dunne, E. M., Rondo, L., Downard, A., Bianchi, F., Kupc, A., Tsagkogeorgas, G., Lehtipalo, K., Manninen, H. E., Almeida, J., Amorim, A., Wagner, P. E., Hansel, A., Kirkby, J., Kürten, A., Donahue, N. M., Makhmutov, V., Mathot, S., Metzger, A., Petäjä, T., Schnitzhofer, R., Sipilä, M., Stozhkov, Y., Tomé, A., Kerminen, V.-M., Carslaw, K., Curtius, J., Baltensperger, U., and Kulmala, M.: Experimental investigation of ion–ion recombination under atmospheric conditions, Atmos. Chem. Phys., 15, 7203–7216, https://doi.org/10.5194/acp-15-7203-2015, 2015.

Fuchs, N. A.: On the stationary charge distribution on aerosol particles in a bipolar ionic atmosphere, Geofisica Pura e Applicata, 56, 185–193, https://doi.org/10.1007/BF01993343, 1963.

Gatti, M. and Kortshagen, U.: Analytical model of particle charging in plasmas over a wide range of collisionality, Phys. Rev. E, 78, 046402, https://doi.org/10.1103/PhysRevE.78.046402, 2008.

Gopalakrishnan, R. and Hogan, C. J.: Coulomb-influenced collisions in aerosols and dusty plasmas, Phys. Rev. E, 85, 026410, https://doi.org/10.1103/PhysRevE.85.026410, 2012.

Gopalakrishnan, R., Meredith, M. J., Larriba-Andaluz, C., and Hogan, C. J.: Brownian dynamics determination of the bipolar steady state charge distribution on spheres and non-spheres in the transition regime, Journal of Aerosol Science, 63, 126–145, https://doi.org/10.1016/j.jaerosci.2013.04.007, 2013.

Guo, S. and Xue, H.: The enhancement of droplet collision by electric charges and atmospheric electric fields, Atmos. Chem. Phys., 21, 69–85, https://doi.org/10.5194/acp-21-69-2021, 2021.

He, X.-C., Iyer, S., Sipilä, M., Ylisirniö, A., Peltola, M., Kontkanen, J., Baalbaki, R., Simon, M., Kürten, A., Tham, Y. J., Pesonen, J., Ahonen, L. R., Amanatidis, S., Amorim, A., Baccarini, A., Beck, L., Bianchi, F., Brilke, S., Chen, D., Chiu, R., Curtius, J., Dada, L., Dias, A., Dommen, J., Donahue, N. M., Duplissy, J., El Haddad, I., Finkenzeller, H., Fischer, L., Heinritzi, M., Hofbauer, V., Kangasluoma, J., Kim, C., Koenig, T. K., Kubečka, J., Kvashnin, A., Lamkaddam, H., Lee, C. P., Leiminger, M., Li, Z., Makhmutov, V., Xiao, M., Marten, R., Nie, W., Onnela, A., Partoll, E., Petäjä, T., Salo, V.-T., Schuchmann, S., Steiner, G., Stolzenburg, D., Stozhkov, Y., Tauber, C., Tomé, A., Väisänen, O., Vazquez-Pufleau, M., Volkamer, R., Wagner,

A. C., Wang, M., Wang, Y., Wimmer, D., Winkler, P. M., Worsnop, D. R., Wu, Y., Yan, C., Ye, Q., Lehtinen, K., Nieminen, T., Manninen, H. E., Rissanen, M., Schobesberger, S., Lehtipalo, K., Baltensperger, U., Hansel, A., Kerminen, V.-M., Flagan, R. C., Kirkby, J., Kurtén, T., and Kulmala, M.: Determination of the collision rate coefficient between charged iodic acid clusters and iodic acid using the appearance time method, Aerosol Science and Technology, 55, 231–242, https://doi.org/10.1080/02786826.2020.1839013, 2021.

Hogan, C. J. and de la Mora, J. F.: Ion Mobility Measurements of Nondenatured 12–150 kDa Proteins and Protein Multimers by Tandem Differential Mobility Analysis–Mass Spectrometry (DMA-MS), J. Am. Soc. Mass Spectrom., 22, 158–172, https://doi.org/10.1007/s13361-010-0014-7, 2011.

Hoppel, W. A. and Frick, G. M.: Ion—Aerosol Attachment Coefficients and the Steady-State Charge Distribution on Aerosols in a Bipolar Ion Environment, Aerosol Science and Technology, 5, 1–21, https://doi.org/10.1080/02786828608959073, 1986.

Intergovernmental Panel on Climate Change (Ed.): Climate Change 2013 - The Physical Science Basis: Working Group I Contribution to the Fifth Assessment Report of the Intergovernmental Panel on Climate Change, Cambridge University Press, Cambridge, https://doi.org/10.1017/CBO9781107415324, 2014a.

Intergovernmental Panel on Climate Change (Ed.): Clouds and Aerosols, in: Climate Change 2013 - The Physical Science Basis, Cambridge University Press, Cambridge, 571–658, https://doi.org/10.1017/CBO9781107415324.016, 2014b.

Kangasluoma, J. and Kontkanen, J.: On the sources of uncertainty in the sub-3 nm particle concentration measurement, Journal of Aerosol Science, 112, 34–51, https://doi.org/10.1016/j.jaerosci.2017.07.002, 2017.

Kangasluoma, J., Cai, R., Jiang, J., Deng, C., Stolzenburg, D., Ahonen, L. R., Chan, T., Fu, Y., Kim, C., Laurila, T. M., Zhou, Y., Dada, L., Sulo, J., Flagan, R. C., Kulmala, M., Petäjä, T., and Lehtipalo, K.: Overview of measurements and current instrumentation for 1–10 nm aerosol particle number size distributions, Journal of Aerosol Science, 148, 105584, https://doi.org/10.1016/j.jaerosci.2020.105584, 2020.

Kebarle, P. and Verkerk, U. H.: Electrospray: From ions in solution to ions in the gas phase, what we know now, Mass Spectrom. Rev., 28, 898–917, https://doi.org/10.1002/mas.20247, 2009.

Kirkby, J., Curtius, J., Almeida, J., Dunne, E., Duplissy, J., Ehrhart, S., Franchin, A., Gagné, S., Ickes, L., Kürten, A., Kupc, A., Metzger, A., Riccobono, F., Rondo, L., Schobesberger, S., Tsagkogeorgas, G., Wimmer, D., Amorim, A., Bianchi, F., Breitenlechner, M., David, A., Dommen, J., Downard, A., Ehn, M., Flagan, R. C., Haider, S., Hansel, A., Hauser, D., Jud, W., Junninen, H., Kreissl, F., Kvashin, A., Laaksonen, A., Lehtipalo, K., Lima, J., Lovejoy, E. R., Makhmutov, V., Mathot, S., Mikkilä, J., Minginette, P., Mogo, S., Nieminen, T., Onnela, A., Pereira, P., Petäjä, T., Schnitzhofer, R., Seinfeld, J. H., Sipilä, M., Stozhkov, Y., Stratmann, F., Tomé, A., Vanhanen, J., Viisanen, Y., Vrtala, A., Wagner, P. E., Walther, H., Weingartner, E., Wex, H., Winkler, P. M., Carslaw, K. S., Worsnop, D. R., Baltensperger, U., and Kulmala, M.: Role of sulphuric acid, ammonia and galactic cosmic rays in atmospheric aerosol nucleation, Nature, 476, 429–433, https://doi.org/10.1038/nature10343, 2011.

Kirkby, J., Duplissy, J., Sengupta, K., Frege, C., Gordon, H., Williamson, C., Heinritzi, M., Simon, M., Yan, C., Almeida, J., Tröstl, J., Nieminen, T., Ortega, I. K., Wagner, R., Adamov, A., Amorim, A., Bernhammer, A.-K., Bianchi, F., Breitenlechner, M., Brilke, S., Chen, X., Craven, J., Dias, A., Ehrhart, S., Flagan, R. C., Franchin, A., Fuchs, C., Guida, R., Hakala, J., Hoyle, C. R., Jokinen, T., Junninen, H., Kangasluoma, J., Kim, J., Krapf, M., Kürten, A., Laaksonen, A., Lehtipalo, K., Makhmutov, V., Mathot, S., Molteni, U., Onnela, A., Peräkylä, O., Piel, F., Petäjä, T., Praplan, A. P., Pringle, K., Rap, A., Richards, N. A. D., Riipinen, I., Rissanen, M. P., Rondo, L., Sarnela, N., Schobesberger, S., Scott, C. E., Seinfeld, J. H., Sipilä, M., Steiner, G., Stozhkov, Y., Stratmann, F., Tomé, A., Virtanen, A., Vogel, A. L., Wagner, A. C., Wagner, P. E., Weingartner, E., Wimmer, D., Winkler, P. M., Ye, P., Zhang, X., Hansel, A., Dommen, J., Donahue, N. M., Worsnop, D. R., Baltensperger, U.,

Kulmala, M., Carslaw, K. S., and Curtius, J.: Ion-induced nucleation of pure biogenic particles, Nature, 533, 521–526, https://doi.org/10.1038/nature17953, 2016.

595   Ku, B. K. and de la Mora, J. F.: Relation between Electrical Mobility, Mass, and Size for Nanodrops 1–6.5 nm in Diameter in Air, Aerosol Science and Technology, 43, 241–249, https://doi.org/10.1080/02786820802590510, 2009.

Kulmala, M., Kerminen, V.-M., Petäjä, T., Ding, A. J., and Wang, L.: Atmospheric gas-to-particle conversion: why NPF events are observed in megacities?, Faraday Discuss., 200, 271–288, https://doi.org/10.1039/C6FD00257A, 2017.

Kupc, A., Amorim, A., Curtius, J., Danielczok, A., Duplissy, J., Ehrhart, S., Walther, H., Ickes, L., Kirkby, J., Kürten, A.,
600   Lima, J. M., Mathot, S., Minginette, P., Onnela, A., Rondo, L., and Wagner, P. E.: A fibre-optic UV system for H2SO4 production in aerosol chambers causing minimal thermal effects, Journal of Aerosol Science, 42, 532–543, https://doi.org/10.1016/j.jaerosci.2011.05.001, 2011.

Kürten, A., Rondo, L., Ehrhart, S., and Curtius, J.: Performance of a corona ion source for measurement of sulfuric acid by chemical ionization mass spectrometry, Atmos. Meas. Tech., 4, 437–443, https://doi.org/10.5194/amt-4-437-2011, 2011.

605   Kürten, A., Rondo, L., Ehrhart, S., and Curtius, J.: Calibration of a Chemical Ionization Mass Spectrometer for the Measurement of Gaseous Sulfuric Acid, J. Phys. Chem. A, 116, 6375–6386, https://doi.org/10.1021/jp212123n, 2012.

Kürten, A., Jokinen, T., Simon, M., Sipilä, M., Sarnela, N., Junninen, H., Adamov, A., Almeida, J., Amorim, A., Bianchi, F., Breitenlechner, M., Dommen, J., Donahue, N. M., Duplissy, J., Ehrhart, S., Flagan, R. C., Franchin, A., Hakala, J., Hansel, A., Heinritzi, M., Hutterli, M., Kangasluoma, J., Kirkby, J., Laaksonen, A., Lehtipalo, K., Leiminger, M., Makhmutov, V., Mathot,
610   S., Onnela, A., Petäjä, T., Praplan, A. P., Riccobono, F., Rissanen, M. P., Rondo, L., Schobesberger, S., Seinfeld, J. H., Steiner, G., Tomé, A., Tröstl, J., Winkler, P. M., Williamson, C., Wimmer, D., Ye, P., Baltensperger, U., Carslaw, K. S., Kulmala, M., Worsnop, D. R., and Curtius, J.: Neutral molecular cluster formation of sulfuric acid–dimethylamine observed in real time under atmospheric conditions, Proc. Natl. Acad. Sci. U.S.A., 111, 15019–15024, https://doi.org/10.1073/pnas.1404853111, 2014.

615   Larriba, C., Hogan, C. J., Attoui, M., Borrajo, R., Garcia, J. F., and de la Mora, J. F.: The Mobility–Volume Relationship below 3.0 nm Examined by Tandem Mobility–Mass Measurement, Aerosol Science and Technology, 45, 453–467, https://doi.org/10.1080/02786826.2010.546820, 2011.

Lehtinen, K. E. J. and Kulmala, M.: A model for particle formation and growth in the atmosphere with molecular resolution in size, Atmos. Chem. Phys., 3, 251–257, https://doi.org/10.5194/acp-3-251-2003, 2003.

620   Lehtipalo, K., Leppä, Johannes, Kontkanen, J., Kangasluoma, J., Franchin, A., Wimmer, D., Schobesberger, S., Junninen, H., Petäjä, T., Sipilä, M., Mikkilä, J., Vanhanen, J., Worsnop, D. R., and Kulmala, M.: Methods for determining particle size distribution and growth rates between 1 and 3 nm using the Particle Size Magnifier, Boreal Environment Research, 19, 215–236, 2014.

Liu, W., Kaufman, S. L., Osmondson, B. L., Sem, G. J., Quant, F. R., and Oberreit, D. R.: Water-Based Condensation Particle
625   Counters for Environmental Monitoring of Ultrafine Particles, Journal of the Air & Waste Management Association, 56, 444–455, https://doi.org/10.1080/10473289.2006.10464520, 2006.

López-Herrera, J. M., Barrero, A., Boucard, A., Loscertales, I. G., and Márquez, M.: An experimental study of the electrospraying of water in air at atmospheric pressure, J. Am. Soc. Mass Spectrom., 15, 253–259, https://doi.org/10.1016/j.jasms.2003.10.018, 2004.

630 López-Yglesias, X. and Flagan, R. C.: Ion–Aerosol Flux Coefficients and the Steady-State Charge Distribution of Aerosols in a Bipolar Ion Environment, Aerosol Science and Technology, 47, 688–704, https://doi.org/10.1080/02786826.2013.783684, 2013.

Mahfouz, N. G. A. and Donahue, N. M.: Atmospheric Nanoparticle Survivability Reduction Due to Charge-Induced Coagulation Scavenging Enhancement, Geophys Res Lett, 48, https://doi.org/10.1029/2021GL092758, 2021a.

635 Mahfouz, N. G. A. and Donahue, N. M.: Technical note: The enhancement limit of coagulation scavenging of small charged particles, Atmos. Chem. Phys., 21, 3827–3832, https://doi.org/10.5194/acp-21-3827-2021, 2021b.

Mahfouz, N. G. A., Gorkowski, K. J., Chuang, W. K., and Kumar, A.: particula: v0.0.7, , https://doi.org/10.5281/ZENODO.6634653, 2022.

Manninen, H. E., Petäjä, T., Asmi, E., Riipinen, I., Nieminen, T., Mikkilä, J., Hörrak, U., Mirme, A., Mirme, S., Laakso, L.,
640 Kerminen, V.-M., and Kulmala, M.: Long-term field measurements of charged and neutral clusters using Neutral cluster and Air Ion Spectrometer (NAIS), Boreal Environment Research, 14, 591–605, 2009.

Manninen, H. E., Mirme, S., Mirme, A., Petäjä, T., and Kulmala, M.: How to reliably detect molecular clusters and nucleation mode particles with Neutral cluster and Air Ion Spectrometer (NAIS), Atmos. Meas. Tech., 9, 3577–3605, https://doi.org/10.5194/amt-9-3577-2016, 2016.

645 Marginean, I., Kelly, R. T., Prior, D. C., LaMarche, B. L., Tang, K., and Smith, R. D.: Analytical Characterization of the Electrospray Ion Source in the Nanoflow Regime, Anal. Chem., 80, 6573–6579, https://doi.org/10.1021/ac800683s, 2008.

Marten, R., Xiao, M., Rörup, B., Wang, M., Kong, W., He, X.-C., Stolzenburg, D., Pfeifer, J., Marie, G., Wang, D. S., Scholz, W., Baccarini, A., Lee, C. P., Amorim, A., Baalbaki, R., Bell, D. M., Bertozzi, B., Caudillo, L., Chu, B., Dada, L., Duplissy, J., Finkenzeller, H., Carracedo, L. G., Granzin, M., Hansel, A., Heinritzi, M., Hofbauer, V., Kemppainen, D., Kürten, A.,
650 Lampimäki, M., Lehtipalo, K., Makhmutov, V., Manninen, H. E., Mentler, B., Petäjä, T., Philippov, M., Shen, J., Simon, M., Stozhkov, Y., Tomé, A., Wagner, A. C., Wang, Y., Weber, S. K., Wu, Y., Zauner-Wieczorek, M., Curtius, J., Kulmala, M., Möhler, O., Volkamer, R., Winkler, P. M., Worsnop, D. R., Dommen, J., Flagan, R. C., Kirkby, J., Donahue, N. M., Lamkaddam, H., Baltensperger, U., and El Haddad, I.: Survival of newly formed particles in haze conditions, Environmental Science: Atmospheres, 2, 491–499, https://doi.org/10.5445/IR/1000146549, 2022.

655 Metzger, A., Verheggen, B., Dommen, J., Duplissy, J., Prevot, A. S. H., Weingartner, E., Riipinen, I., Kulmala, M., Spracklen, D. V., Carslaw, K. S., and Baltensperger, U.: Evidence for the role of organics in aerosol particle formation under atmospheric conditions, Proceedings of the National Academy of Sciences, 107, 6646–6651, https://doi.org/10.1073/pnas.0911330107, 2010.

Mirme, A., Tamm, E., Mordas, G., Vana, M., Uin, J., Mirme, S., Bernotas, T., Laakso, L., Hirsikko, A., and Kulmala, M.: A
660 wide-range multi-channel Air Ion Spectrometer, Boreal Environment Research, 12, 247–264, 2007.

Mirme, S. and Mirme, A.: The mathematical principles and design of the NAIS – a spectrometer for the measurement of cluster ion and nanometer aerosol size distributions, Atmos. Meas. Tech., 6, 1061–1071, https://doi.org/10.5194/amt-6-1061-2013, 2013.

Murphy, D. M. and Koop, T.: Review of the vapour pressures of ice and supercooled water for atmospheric applications, Q.
665 J. R. Meteorol. Soc., 131, 1539–1565, https://doi.org/10.1256/qj.04.94, 2005.

Myhre, C. E. L., Nielsen, C. J., and Saastad, O. W.: Density and Surface Tension of Aqueous H_2SO_4 at Low Temperature, J. Chem. Eng. Data, 43, 617–622, https://doi.org/10.1021/je980013g, 1998.

Nieminen, T., Lehtinen, K. E. J., and Kulmala, M.: Sub-10 nm particle growth by vapor condensation – effects of vapor molecule size and particle thermal speed, Atmos. Chem. Phys., 10, 9773–9779, https://doi.org/10.5194/acp-10-9773-2010, 670 2010.

Ouyang, H., Gopalakrishnan, R., and Hogan, C. J.: Nanoparticle collisions in the gas phase in the presence of singular contact potentials, The Journal of Chemical Physics, 137, 064316, https://doi.org/10.1063/1.4742064, 2012.

Pfeifer, J., Simon, M., Heinritzi, M., Piel, F., Weitz, L., Wang, D., Granzin, M., Müller, T., Bräkling, S., Kirkby, J., Curtius, J., and Kürten, A.: Measurement of ammonia, amines and iodine compounds using protonated water cluster chemical 675 ionization mass spectrometry, Atmos. Meas. Tech., 13, 2501–2522, https://doi.org/10.5194/amt-13-2501-2020, 2020.

Rayleigh, Lord: XX. *On the equilibrium of liquid conducting masses charged with electricity*, The London, Edinburgh, and Dublin Philosophical Magazine and Journal of Science, 14, 184–186, https://doi.org/10.1080/14786448208628425, 1882.

Seinfeld, J. H. and Pandis, S. N.: Atmospheric chemistry and physics: from air pollution to climate change, Third edition., John Wiley & Sons, Hoboken, New Jersey, 1120 pp., 2016.

680 Simon, M., Heinritzi, M., Herzog, S., Leiminger, M., Bianchi, F., Praplan, A., Dommen, J., Curtius, J., and Kürten, A.: Detection of dimethylamine in the low pptv range using nitrate chemical ionization atmospheric pressure interface time-of-flight (CI-APi-TOF) mass spectrometry, Atmos. Meas. Tech., 9, 2135–2145, https://doi.org/10.5194/amt-9-2135-2016, 2016.

Skrotzki, J.: High-accuracy multiphase humidity measurements using TDLAS: application to the investigation of ice growth in simulated cirrus clouds, https://doi.org/10.11588/HEIDOK.00013141, 2012.

685 Smith, J. N., Flagan, R. C., and Beauchamp, J. L.: Droplet Evaporation and Discharge Dynamics in Electrospray Ionization, J. Phys. Chem. A, 106, 9957–9967, https://doi.org/10.1021/jp025723e, 2002.

Sterling, H. J., Cassou, C. A., Trnka, M. J., Burlingame, A. L., Krantz, B. A., and Williams, E. R.: The role of conformational flexibility on protein supercharging in native electrospray ionization, Phys. Chem. Chem. Phys., 13, 18288, https://doi.org/10.1039/c1cp20277d, 2011.

690 Stolzenburg, D., Simon, M., Ranjithkumar, A., Kürten, A., Lehtipalo, K., Gordon, H., Ehrhart, S., Finkenzeller, H., Pichelstorfer, L., Nieminen, T., He, X.-C., Brilke, S., Xiao, M., Amorim, A., Baalbaki, R., Baccarini, A., Beck, L., Bräkling, S., Caudillo Murillo, L., Chen, D., Chu, B., Dada, L., Dias, A., Dommen, J., Duplissy, J., El Haddad, I., Fischer, L., Gonzalez Carracedo, L., Heinritzi, M., Kim, C., Koenig, T. K., Kong, W., Lamkaddam, H., Lee, C. P., Leiminger, M., Li, Z., Makhmutov, V., Manninen, H. E., Marie, G., Marten, R., Müller, T., Nie, W., Partoll, E., Petäjä, T., Pfeifer, J., Philippov, M., 695 Rissanen, M. P., Rörup, B., Schobesberger, S., Schuchmann, S., Shen, J., Sipilä, M., Steiner, G., Stozhkov, Y., Tauber, C., Tham, Y. J., Tomé, A., Vazquez-Pufleau, M., Wagner, A. C., Wang, M., Wang, Y., Weber, S. K., Wimmer, D., Wlasits, P. J., Wu, Y., Ye, Q., Zauner-Wieczorek, M., Baltensperger, U., Carslaw, K. S., Curtius, J., Donahue, N. M., Flagan, R. C., Hansel, A., Kulmala, M., Lelieveld, J., Volkamer, R., Kirkby, J., and Winkler, P. M.: Enhanced growth rate of atmospheric particles from sulfuric acid, Atmos. Chem. Phys., 20, 7359–7372, https://doi.org/10.5194/acp-20-7359-2020, 2020.

700 Suresh, V., Li, L., Redmond Go Felipe, J., and Gopalakrishnan, R.: Modeling nanoparticle charge distribution in the afterglow of non-thermal plasmas and comparison with measurements, J. Phys. D: Appl. Phys., 54, 275205, https://doi.org/10.1088/1361-6463/abf70c, 2021.

Tamadate, T., Higashi, H., Seto, T., and Hogan, C. J.: Calculation of the ion–ion recombination rate coefficient via a hybrid continuum-molecular dynamics approach, J. Chem. Phys., 152, 094306, https://doi.org/10.1063/1.5144772, 2020a.

705   Tamadate, T., Higashi, H., Hogan, C. J., and Seto, T.: The charge reduction rate for multiply charged polymer ions *via* ion–ion recombination at atmospheric pressure, Phys. Chem. Chem. Phys., 22, 25215–25226, https://doi.org/10.1039/D0CP03989F, 2020b.

Tikhonov, A. N.: Solution of incorrectly formulated problem and the regularization method, Soviet Math. Dokl, 4, 1035–1038, 1963.

710   Tinsley, B. A.: Uncertainties in Evaluating Global Electric Circuit Interactions With Atmospheric Clouds and Aerosols, and Consequences for Radiation and Dynamics, JGR Atmospheres, 127, e2021JD035954, https://doi.org/10.1029/2021JD035954, 2022.

Tinsley, B. A., Rohrbaugh, R. P., Hei, M., and Beard, K. V.: Effects of Image Charges on the Scavenging of Aerosol Particles by Cloud Droplets and on Droplet Charging and Possible Ice Nucleation Processes, J. Atmos. Sci., 57, 2118–2134,
715   https://doi.org/10.1175/1520-0469(2000)057<2118:EOICOT>2.0.CO;2, 2000.

Tritscher, T., Beeston, M., Zerrath, A. F., Elzey, S., Krinke, T. J., Filimundi, E., and Bischof, O. F.: NanoScan SMPS – A Novel, Portable Nanoparticle Sizing and Counting Instrument, J. Phys.: Conf. Ser., 429, 012061, https://doi.org/10.1088/1742-6596/429/1/012061, 2013.

Turco, R. P., Zhao, J.-X., and Yu, F.: A new source of tropospheric aerosols: Ion-ion recombination, Geophys. Res. Lett., 25,
720   635–638, https://doi.org/10.1029/98GL00253, 1998.

Vanhanen, J., Mikkilä, J., Lehtipalo, K., Sipilä, M., Manninen, H. E., Siivola, E., Petäjä, T., and Kulmala, M.: Particle Size Magnifier for Nano-CN Detection, Aerosol Science and Technology, 45, 533–542, https://doi.org/10.1080/02786826.2010.547889, 2011.

Vehkamäki, H., Kulmala., M., Napari, I., Lehtinen, K. E. J., Timmreck, M., Noppel, M., and Laaksonen, A.: An improved
725   parameterization for sulfuric acid–water nucleation rates for tropospheric and stratospheric conditions, J. Geophys. Res., 107, AAC 3-1-AAC 3-10, https://doi.org/10.1029/2002JD002184, 2002.

Wang, M., He, X.-C., Finkenzeller, H., Iyer, S., Chen, D., Shen, J., Simon, M., Hofbauer, V., Kirkby, J., Curtius, J., Maier, N., Kurtén, T., Worsnop, D. R., Kulmala, M., Rissanen, M., Volkamer, R., Tham, Y. J., Donahue, N. M., and Sipilä, M.: Measurement of iodine species and sulfuric acid using bromide chemical ionization mass spectrometers, Atmos. Meas. Tech.,
730   14, 4187–4202, https://doi.org/10.5194/amt-14-4187-2021, 2021.

Wiedensohler, A.: An approximation of the bipolar charge distribution for particles in the submicron size range, Journal of Aerosol Science, 19, 387–389, https://doi.org/10.1016/0021-8502(88)90278-9, 1988.

Wiedensohler, A., Birmili, W., Nowak, A., Sonntag, A., Weinhold, K., Merkel, M., Wehner, B., Tuch, T., Pfeifer, S., Fiebig, M., Fjäraa, A. M., Asmi, E., Sellegri, K., Depuy, R., Venzac, H., Villani, P., Laj, P., Aalto, P., Ogren, J. A., Swietlicki, E.,
735   Williams, P., Roldin, P., Quincey, P., Hüglin, C., Fierz-Schmidhauser, R., Gysel, M., Weingartner, E., Riccobono, F., Santos, S., Grüning, C., Faloon, K., Beddows, D., Harrison, R., Monahan, C., Jennings, S. G., O'Dowd, C. D., Marinoni, A., Horn, H.-G., Keck, L., Jiang, J., Scheckman, J., McMurry, P. H., Deng, Z., Zhao, C. S., Moerman, M., Henzing, B., de Leeuw, G., Löschau, G., and Bastian, S.: Mobility particle size spectrometers: harmonization of technical standards and data structure to facilitate high quality long-term observations of atmospheric particle number size distributions, Atmos. Meas. Tech., 5, 657–
740   685, https://doi.org/10.5194/amt-5-657-2012, 2012.

Winklmayr, W., Reischl, G. P., Lindner, A. O., and Berner, A.: A new electromobility spectrometer for the measurement of aerosol size distributions in the size range from 1 to 1000 nm, Journal of Aerosol Science, 22, 289–296, https://doi.org/10.1016/S0021-8502(05)80007-2, 1991.

Zeleny, J.: The velocity of the ions produced in gases by Röntgen rays, Proc. R. Soc. Lond., 66, 238–241, https://doi.org/10.1098/rspl.1899.0095, 1900.

Zhou, L. and Tinsley, B. A.: Production of space charge at the boundaries of layer clouds, J. Geophys. Res., 112, D11203, https://doi.org/10.1029/2006JD007998, 2007.